

Digital light processing based additive manufacturing of resin bonded SiC grinding wheels and their grinding performance

Qingfeng Ai (✉ aq@hs-furtwangen.de)

Institute of Precision Machining KSF

Jahangir Khosravi

Institute of Precision Machining KSF

Bahman Azarhoushang

Institute of Precision Machining KSF

Amir Daneshi

Institute of Precision Machining KSF

Björn Becker

Institute of Precision Machining KSF

Research Article

Keywords: Grinding tool, additive manufactured grinding tool, Digital light processing, Grinding, Grinding tool wear

Posted Date: June 25th, 2021

DOI: <https://doi.org/10.21203/rs.3.rs-358806/v1>

License:  This work is licensed under a Creative Commons Attribution 4.0 International License.

[Read Full License](#)

Version of Record: A version of this preprint was published at The International Journal of Advanced Manufacturing Technology on September 21st, 2021. See the published version at <https://doi.org/10.1007/s00170-021-08016-z>.

Abstract

In this study, an additive manufacturing process based on digital light processing was employed for quick, flexible, and economical fabrication of resin-bonded SiC grinding tools. The grinding wheel has been fabricated using laboratory manufacturing processes that utilize ultraviolet-curable resins and conventional abrasives. Also, desirable geometries and features like integrated coolant holes, which are difficult or even almost impossible to manufacture by conventional processes, are easily achievable. Grinding experiments were carried out by different process parameters, and with two different grinding wheels, i.e. with and without cooling channels with different concentrations (25 wt.% and 50 wt.% grains) to evaluate the grinding efficiency of the produced tools. Grinding forces, tool wear, tool loading, and ground surface quality were measured and analyzed. The wear rates of the grinding wheels with cooling channels were generally less than those without cooling channels, particularly in the deep grinding processes with large contact areas. Grinding tests on a hardened steel have shown that the integration of cooling lubricant channels almost prevents the wheel loading. In addition, by increasing the cutting speed (from 15 to 30 m/s) and decreasing the feed rate (from 10 to 2 m/min) the grinding wheel wear was significantly reduced. Furthermore, surface grinding of aluminum resulted in surface roughness values (Ra) in the range of 1 μm to 2.5 μm , while a Ra of about 0.2 μm was achieved by grinding hardened steel (100Cr6) with the same grinding conditions. Using the higher SiC-grain concentration (50 wt.%), it was determined that the surface roughness was 50% finer. Additionally the tool wear was significantly reduced (up to 30 times depending on the process parameters). The wear characteristics of the grinding wheel was analyzed through a novel image processing system. Significant correlations were found between wear flat of grains and the increase in grinding forces due to the tool wear.

1. Introduction

Resin-bonded abrasive cutting tools including grinding wheels, lapping plates, and even polishing pads are widely applied in industry due to their advantages in low process forces and self-sharpening properties [1]. Resin bonded abrasive tools are generally manufactured in thermal-pressing molds. Most of the manufacturing process needs high pressure and high temperatures (of about 200 °C) for a long time [2]. The required profile of the grinding wheels can be achieved by providing appropriate molds. As an alternative, it can also be conditioned with different conditioning tools to produce a specific profile. To improve the grinding performance, different structures can be created on the grinding tools by mechanical processes [3] or laser ablation [4–6]. In addition to the high cost and time required, there are also some technical limits on creating profiles and structures (textures) using secondary conditioning methods. For example, complex geometries such as concave shapes, structures with large aspect-ratios, or internal structures are not feasible with this manufacturing process.

The additive manufacturing (AM) process is known to be a flexible manufacturing process for complex geometries, and it has recently been developed with many novel applications in engineering. Bikas et al. [7] provided a method to evaluate and select a proper process of additive manufacturing and discussed not only whether AM would be usable for a specific part, but gave details regarding selecting a

corresponding AM process. In this regard, AM technology has recently been in the focus of several research studies as an alternative for the conventional manufacturing process of both metal bonded and resin bonded abrasive cutting tools. Tian et al. [8] additively fabricated porous metal bonded grinding wheels based on the selective laser melting (SLM) technology. Grinding wheels with octahedron structure and honeycomb structures were fabricated in a way so that porous metal bonded grinding wheels with controllable pore shape, size, quantity, distribution, and high porosity could be realized. The holes and structures play a very crucial role in porosity. Pore structure and porosity can be controlled very accurately. This has clear advantages over the majority of the conventionally produced metal bonded superabrasive grinding wheels which have almost no porosity. Yang et al. [9] also developed an additive manufacturing (AM) technology to fabricate metal bonded diamond grinding wheels with regular grain distribution. For the resin bonded cutting tools Du et al. [10] printed grinding wheels of polyamide (nylon) and diamond grains using a selective laser-sintering process while investigating their properties. The results indicated a good adhesion of plastics but also showed the problem of nylon melting during the grinding process and forming a smearing layer on the ground surface. Most thermoplastic materials have a melting point of less than 180°C. When the cutting temperature increases during the grinding, the material will begin to melt and consequently become smeary. This is the reason why most thermoplastics are not used as the binding material. Therefore, thermosetting resin is the most common bonding material for resin bonded grinding wheels. For example, common resins are phenol formaldehyde, novolac phenolics and especially those with added crosslinking agent (e.g., hexa-methylenetetramine), phenoplasts, aminoplasts, vinyl ester resins, alkyd resins, allyl resins, furan resins, epoxies, polyurethanes, cyanate esters, and polyimides [11]. Generally, these materials have higher mechanical and thermal properties than thermoplastics. When subjected to high temperature and pressure, they do not melt and so do not become smeary. Hence, some researchers focused mainly on improving the properties of thermosetting resins utilizing various additives [12]. As a subgroup of thermosetting, ultraviolet (UV) light-curable resin has also been investigated by several works. Unlike conventional processes which use heat to evaporate water or solvents from a material, UV curing offers many benefits, including lower energy consumption, excellent film quality, and high processing productivity [13,14]. Chattopadhyay [15] studied the thermal and mechanical properties of different resins (combination of acrylate with epoxy resin, polyurethane and polyester). Some UV resins have similar properties to phenolic resins and can therefore be used as binders in abrasive tools. UV resin bonded abrasive tools have recently been developed and manufactured by stereolithography processes. Such tools have been proved to have substantial advantages over conventional abrasive tools [16,17]. Guo und Du et al [10,18] used a strong ultraviolet-curable resin bond for a diamond lapping plate and compared it with a conventionally manufactured lapping plate. The results showed not only a higher material removal rate but also a finer surface. In [19] the effect of different additive particles on the performance of ultraviolet-cured resin bond grinding wheels was studied. The holding force of resin with 15 wt.% Al₂O₃ addition was found to be higher than that of pure UV resin. The Grinding experiment demonstrated the performance of UV resinoid grinding wheels was therefore significantly improved with the addition of particles. Photopolymers with or without particles hardened by stereolithography (UV resin) are able to efficiently fix the abrasive grains.

However, the previous studies were only based on stereolithography of UV-curable resin. In all the above-mentioned studies, either a profiling tool was used, where the UV resin was injected and hardened in layers, or thin layers of resin were manually applied to a base plate and hardened. The geometry of the molded parts can usually only be achieved by a specially designed mold and therefore is very limited. The production of complex geometries is not possible by this method. The advantage of additive manufacturing is not fully explored in the manufacturing processes described above.

The Digital Light Processing (DLP) additive manufacturing process has quickly been accepted as the process of two-dimensional stereolithography printing. In this process, the single thin layers of resin material, which are fixed on a moving plate, are hardened through a short time exposure to single sectional lights. During the printing process, the print platform moves upwards out of the liquid layer by layer, gradually creating a solid structure with the desired shape. In this 3D printing process, no mold tool is required to create the geometry and different shaped parts can be flexibly produced directly from the CAD files.

There is almost no report (according to authors knowledge) about utilizing the DLP process in manufacturing of abrasive tools. The novel idea of the present research was the use of the projection technology for the additive production of UV resin bonded grinding tools.

This manufacturing process offers the maximum flexibility in the production of grinding tools. By direct exposure with corresponding patterns, the freely selected target geometry can be generated. In addition to defined profiles and structures, the specification of the grinding wheel (grit type, size and concentration) can be selected individually based on requirements. Also, special structures, profiles or cooling channels, which are difficult or impossible to produce with conventional methods, can simply be created without the need for costly and time intensive subsequent conditioning processes, especially for expensive superabrasive grinding wheels. Further key economic benefits of this 3D printing process include eliminating the pressing tools and molds, which is required by long-time high-temperature pressing in conventional manufacturing. In addition, ultraviolet curable resin offers some economic advantages over thermal curable resin (in conventional hot press), including a faster curing process in a shorter time with high processing productivity, lower energy consumption, environmental compatibility as it is less harmful for humans and the environment [15,20].

Due to the advantages mentioned above, different UV resin-bonded SiC grinding wheels were produced in KSF using additive DLP manufacturing process and accordingly examined for their grinding performance. Also, special structures in the grinding wheels were printed and their effect was examined. The grinding performance of the additive manufactured grinding wheels, i.e. cutting forces, tool wear and ground surface quality, was quantitatively investigated by surface grinding experiments. Here, the influences of process parameters and different grinding wheel compositions were studied.

2. Materials And Methods

A laboratory manufacturing process was developed for the additive manufacture of resin bonded grinding tools. In order to provide a homogeneous mixture, the abrasive grains and the liquid resin must first be thoroughly mixed together. An electrical mixer with a stainless steel stirring rod is used for this purpose. The viscous mixture was stirred at rotational speed of 200 rpm for 30 minutes. The challenge in processing the liquid material mixture is to prevent segregation of the system. Due to the higher density of the abrasive grains, they sink to the ground in the liquid synthetic resin in only a few minutes. This leads to a nonuniform distribution of the grains in the mixture. To prevent this, an anti-sediment agent is mixed into the liquid mixture, so that the grains remain uniformly distributed in the mixture. Silicon carbide SiC F220 (approx. 60 μm grain size) was used as abrasive grains (Fig. 1). An ultraviolet-curable resin with high mechanical and good thermal properties is used as binder.

The mixture is then filled into a container of a DLP printer. Individual cross-sectional layers of the CAD model were projected onto the transparent bottom of the container. The resin filled with the abrasive particles is hardened layer by layer. The part carrier platform is automatically moved upwards out of the resin mixture in distances equal to the layer thickness after each exposure. For DLP process, we normally use a layer height of 50 to 100 micrometers. In this study, we used 75 micrometer layer height in order to achieve good surface quality and accuracy while at the same time reducing the printing time. The printing time depends on the composition of the mixture, such as the proportion of abrasive grains, grain types, size of the grains, resin bonding, etc. For this mixture, at least 30 seconds for each layer was required. Moreover, we print the first three base layers with a very long exposure time of 300 seconds in order to make it bond well to the printer's platform. Since the hardened surface is not serially scanned with a laser beam, the advantage of the DLP process over stereolithography is a higher production speed. All additive manufactured grinding wheels were rinsed or cleaned with isopropanol and then dried with compressed air. They are then post-processed in a chamber with UV light (405 nm) for one hour to ensure complete curing of the photopolymers and to achieve the final mechanical or thermal properties of the parts. Fig. 2 shows a schematic representation of the additive manufacturing process of the resin bonded abrasive tools.

Cooling lubricant internal channels with a diameter of 0.6 mm have been produced in some of the printed grinding tools so that the cooling lubricant can directly reach the grinding contact zone. This is essential in ensuring that the generated heat in the grinding process can optimally be dissipated. This demonstrates the enormous potential of 3D printing since such hole structures cannot be created using the conventional manufacturing process. Fig. 2 shows examples of freely selected geometries. Hence, defined profiles and structures can be easily created. The accuracy of the DLP process is around 0.1 mm in the printed dimension.

In order to measure the tool wear, a small step was produced on the circumference of the tool. The small step will not take part in the grinding process and will only play the role of a reference surface, which does not change after grinding process. Fig. 3 shows the CAD drawing (left) and the printed disc (right).

Table 1: Specification of 3D printed grinding wheels

Grinding Wheel	SiC F220 (wt.%)	Cooling holes	
		Diameter (mm)	Number
C-50	50	0	0
C-50-K with channels	50	0.6	216
C-25-K with channels	25	0.6	216

Table 1 lists the specifications of the additively manufactured grinding wheels. C-50/C-25 are grinding wheels with 50 respectively 25 weight percent of SiC abrasives, either with (-K) or without cooling channels. Grinding tests with a CNC machining center (Müga R4530) were carried out with the printed wheels to evaluate their properties. Fig. 4 shows the experimental setup of the grinding tests.

Each 3D-printed grinding wheel was dressed prior to the grinding tests with a single grain diamond dresser. Then the workpieces from aluminium or hardened steel (100Cr6, 60 HRC) were ground with different cutting speeds, feed rates and depth of cuts. The experiments were carried out in both reciprocating grinding (shallow depth of cuts and high feed speeds) and deep grinding (high depth of cuts and low feed speeds) strategies. During the dressing and grinding process an emulsion was used for cooling. The grinding forces were measured during the experiments using a Kistler piezoelectric force dynamometer. The process parameters are listed in the table 2.

Table 2: Grinding parameters

Grinding Parameters - reciprocating grinding	
Depth of cut (μm)	10
Cutting speed (m/s)	15, 22, 30
Feed rate (mm/min)	2000, 6000, 10000
Number of passes	1, 5, 25, 50
Coolant-lubricant	Emulsion
Grinding Parameters - deep grinding	
Depth of cut (μm)	100, 200
Cutting speed (m/s)	30
Feed rate (mm/min)	200, 600, 1000
Number of passes	2, 5
Coolant-lubricant	Emulsion
Dressing parameters	
Depth of cut (μm)	2x15 μm
Cutting speed (m/s)	15, 22, 30
Feed rate (mm/min)	231, 339, 462
Overlap ratio	6

To measure the wear (according to J. Verkerk 1976) [21] of the grinding wheel, a thin sheet was ground after certain grinding cycles (Fig. 5). The change in the grinding profile (step height) in this sheet metal was measured (contour measuring device, Hommel-Werke: T-8000) and thus the change in the diameter of the grinding wheel was determined.

The roughness of the ground aluminum block was measured with a tactile roughness measuring device (Hommel-Werke: T-8000). The roughness parameter definition of this device is according to ISO 4287, ISO 13565, and EN 10049, and the cut-off (profile filter) is based on ISO 4288:1998 and ISO 3274:1998. Since our grinding wheel worklength was less than 4 mm, we considered measurement condition as below: Transverse length (l_t) 1.5mm, Evaluation length (l_n) with 1.25mm, Cut-off (λ_c) 0.25mm and Software profile filter (λ_s) 2.5 μ m. For comparison, a hardened steel was also ground as a workpiece and its roughness was measured. A digital microscope (Keyence VHX) and confocal microscope (μ surf mobile plus) were used to inspect the workpieces and tool topographies.

In addition, with a novel digital image processing system [22], the grain condition, the micro- and macro topography of grinding tools after dressing and after grinding were analyzed and the current wear condition or machinability of the grinding wheels were evaluated.

3. Results And Discussion

In the following the quality of the 3d-printed grinding wheels and its performance in the grinding process will be studied:

3.1 3D-printed grinding wheels

Fig. 6 shows an example of the additive-manufactured resin-bonded SiC grinding wheels with 25 wt.% silicon carbide F220 grains. The optical microscopy shows a nearly uniform density of all printed layers. After more than two hours of printing, the grains are still homogeneously distributed and no accumulation of the grains occurred. Fig. 6c with 200x magnification shows the layered structure around printed cooling channel with a diameter of 0.6 mm.

It is interesting to see how the abrasive grains are embedded in the resin during the 3D printing process. Fig. 7 shows how, after DLP printing, most of the grains are fully or partially embedded in the resin. Also, some grains are printed with a large protrusion (Fig. 7b).

In Fig. 8 it can be seen that the coolant is transferred by the cooling channels and tangentially sprayed out. This allows the coolant to directly approach the contact zone and a better cooling-lubricating effect can be achieved.

3.2 Wear

A particularly important factor for an efficient grinding process is the tool wear behavior. To evaluate the photopolymers as bond materials, the wear of the additive manufactured grinding wheels is determined in different material removal volumes, V_w , between 6 and 300 mm³. The grinding wheel was dressed with 10 μm depth of cut and an overlap ratio of 6 at the corresponding cutting speed and prior to the grinding experiments. The wear values for 50 wt.% grains of the printed wheel without cooling holes are shown as a function of cutting speed and feed rate in reciprocating grinding process (Fig. 9 and 10).

As shown in Fig. 9, by increasing the cutting speed the tool wear is significantly reduced. At a cutting speed of 15 m/s after 300 mm³ material removal more than 100 μm radial wear was measured, this value at the cutting speed of 30 m/s reduced to less than 10 μm. As expected, higher cutting speeds positively influence the tool wear because of the reduced chip thickness and therefore there are smaller forces acting on each grain. Additionally, heat dissipation into the grinding wheel possibly reduces due to the shorter contact time between the grains and bond of the grinding wheel with the workpiece surface at higher cutting speeds.

Fig. 10 shows that as anticipated, wear increases significantly with increasing feed rate. When the feed speed is increased from 2000 to 10000 mm/min, the wear on the grinding wheel increases approximately 10 times. This is due to increased chip thickness and thus higher forces acting on each grain and the possibility of reduced cooling and lubrication in the contact zone. The smallest wear overall is hence at maximum cutting speed $v_c=30$ m/s and minimum feed rate $v_{ft}=2000$ mm/min.

The C-50-K additive manufactured grinding wheel with similar dimension and tool specification as the C-50 tool but with additional coolant channels of 0.6 mm diameter, was also tested. The results of surface grinding showed the same trend like the C-50 tool. The wear also increased significantly with decreasing cutting speed or increasing feed rate. Compared to the C-50 wheel, the wear rates of C-50-K tool were in some conditions larger and in other conditions smaller (Fig. 11). At a constant cutting speed of 30 m/s after 300 mm³ material removing, the wear of the C-50-K tool (grinding wheel with cooling channels) was larger at a feed rate of 2000 mm/min than that of the C-50 wheel (without cooling channels). Since, the material removal rate and the induced cutting heat in the contact zone were rather low at these cutting parameters, the amount of abrasive grains plays an important role on the tool wear. However, the wear of C-50-K wheel was significantly lower than the C-50 wheel at feed rates of 6000 and 10000 mm/min. This can be contributed to the high rate of heat generation in the contact zone at higher feed rates, which are taken through the efficient cooling away from the wheel-material contact zone in the case of C-50-K wheel. In other words, the efficiency of the cooling lubricant channels reveals when the heat generation in the grinding is high. On the other hand, compared to the C-50 grinding wheel, the wheel with cooling channels has a smaller abrasive volume and therefore a reduced number of abrasive grains, which can lead to increased wear (due to increased mechanical load on individual grains). This means that a compromise must be made between the advantages and disadvantages of the cooling channels in the tool designation. In some processes, better cooling and lubricating dominates the influence of the smaller number of abrasive grains.

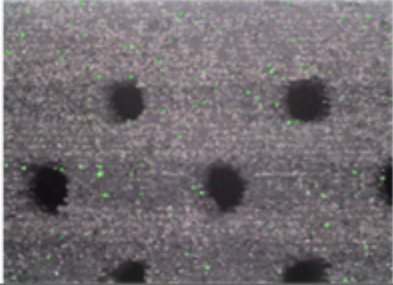
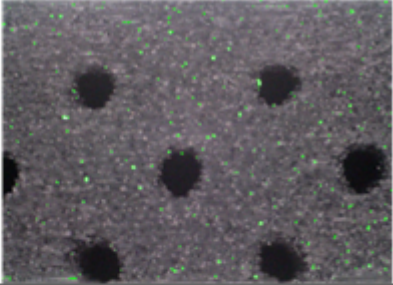
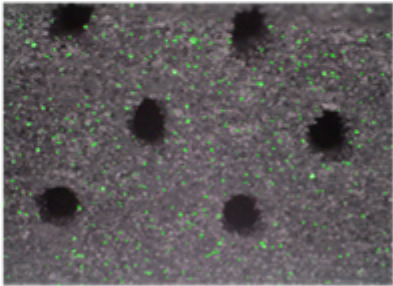
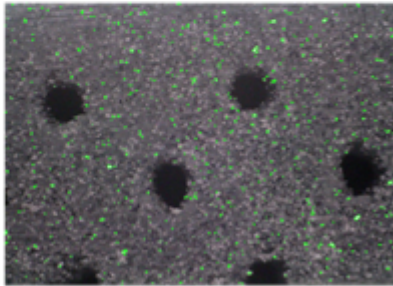
The additive manufactured grinding wheels with and without cooling lubricant channels were also examined in deep grinding. Fig. 12 shows the measured tool wear as a function of the feed rate after 300 mm³ material removal. The advantage of the cooling lubrication channels is obvious here, since the grinding wheel with cooling channels shows significantly less wear than that without cooling channels (C-50). At a feed rate of 200 mm/min, almost no wear was measured on the C-50-K tool, whereas the measured wear on the C-50 wheel was more than 20 µm. The large contact length in the deep grinding leads to a deteriorated cooling and lubrication in the contact zone and significantly higher cutting temperature than the shallow reciprocating surface grinding. During deep grinding with a depth of cut of 100 µm, large cutting forces are acting on each grain and a lot of heat is generated. The integrated cooling channels are particularly effective in removing this heat from the contact zone, ensuring good lubricating and thus reducing the tool wear. This effect can be seen from the corresponding results in Fig. 12. The cooling channels cause also reduction in the normal grinding forces as shown in the same figure. This can be contributed to the smaller number of abrasive grains in the C-50-K grinding wheels due to the presence of the cooling channels. The influence of the efficient cooling on the reduction of tool loading and friction work and hence reduction of grinding forces should not be neglected, as well.

The influence of the process parameters on the wear of the grinding wheels shows the same tendency as conventional manufactured grinding wheels. When comparing grinding wheels with and without cooling channels, it can be seen that the cooling holes can have positive effects when subjected to the high heat generation and large grinding forces.

The wear behavior of the grinding tool is particularly important for an effective grinding process. One of the main wear mechanisms is the flattening of the abrasive grains by friction and abrasion. As grinding tool wear increases, the micro- and eventually the macro-topography of the grinding wheel changes, which influences the process forces [23]. Therefore, a digital image processing system developed by KSF was used to analyze the micro and macro topography of grinding tools and to evaluate the wear condition of the tool. After a few grinding cycles, an image from ground surface was captured and evaluated by an image processing software. Here a certain illumination characteristic is applied to highlight individual surface areas or surface features such as wear-related flattening of the abrasive grains and the reflection of flattened areas. The analysis software recognizes these reflection areas as objects and evaluates them. The reflection portions caused by flattened abrasive grains can be calculated and reported [22]. The measurement of the reflection portion due to flattened abrasive grains took place both after dressing and after the grinding test at different feed rates. The results are summarized in Table 3. The abrasive grains are flattened by polishing or abrasion of the sharp corners and edges. The vertically incident light is reflected by the flattened abrasive grains, which are shown as green areas in the image. After dressing, only a few reflection areas can be seen because the abrasive grains are sharpened. After grinding and as the feed rate increases, the number and the total area of flattened grains increase. At a feed rate of 1000 mm/min most reflections are clearly visible.

Table 3: Measurement of the reflection portion due to flattened abrasive grains after dressing and after the grinding test at different feed rates and the cutting speed of 30 m/s and the

depth of cut of 100 μm

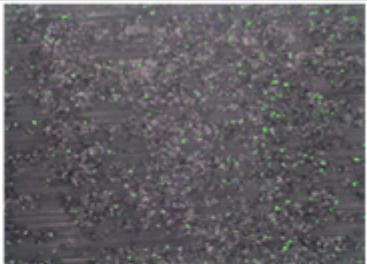
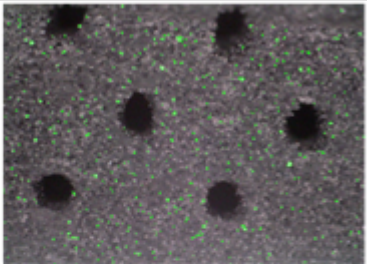
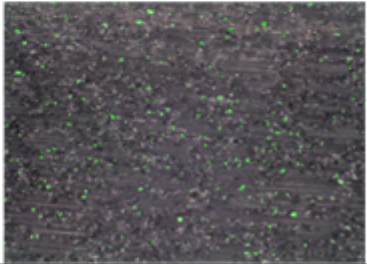
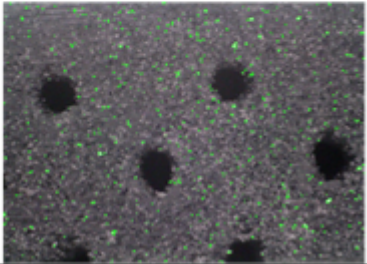
	after dressing	$v_{\text{ft}} = 200 \text{ mm/min}$
		
Amount of flattened grains	186	280
Overall areas of flattened grains	37040 μm^2	78593 μm^2
	$v_{\text{ft}} = 600 \text{ mm/min}$	$v_{\text{ft}} = 1000 \text{ mm/min}$
		
Amount of flattened grains	478	663
Overall areas of flattened grains	109212 μm^2	113801 μm^2

The flattening of the grits leads to an increase in friction and plastic deformation of workpiece material, and thus increasing grinding forces and temperature. During the entire grinding process, the grinding forces were recorded. Fig. 13 shows the results of the number of reflections in connection with the grinding forces for C-50 and C-50-K grinding wheels. The correlation between the reflection portion of each grinding wheel and the grinding forces induced by the same wheel is clearly visible. However, the normal cutting force induced by the C-50 grinding wheel is larger than that of the C-50-K wheel, despite lower amount of flattened grains on this wheel. This is due to the fact that the number of total abrasives of the C-50 wheel are much larger than that of C-50-K wheel (due to the lack of coolant channels). Therefore, the measured amount of flattened abrasives from different grinding wheels cannot be used for comparing the induced cutting forces by these wheels.

The grinding wheel with cooling channels (C-50-K) has a higher number of reflections because more grains are flattened (see Table 4). The reason for this can be explained by the fact that fewer grains are involved in the grinding process on the C-50-K wheel and therefore each individual abrasive grain is subjected to a higher load and therefore more flattened. The lower number of abrasive grains in the C-50-K grinding wheel leads to lower cutting forces (see Fig. 13).

Table 4: Measurement of the reflection portion due to flattened abrasive grains after the grinding test at different feed rates and the cutting speed of 30 m/s and the depth of cut of

100 μm for C-50 and C-50-K grinding wheels

	C - 50	C - 50 - K
$v_{ft} = 600 \text{ mm/min}$		
Amount of flattened grains	291	478
$v_{ft} = 1000 \text{ mm/min}$		
Amount of flattened grains	361	663

3.3 Surface roughness

The long time grinding experiments were followed on the C-50-K wheel with 50% SiC grains (F220) with different process parameters to evaluate the surface roughness of the workpiece. Fig. 14 shows the surface roughness after 300 mm³ material removal for different process parameters.

The surface roughness of the ground workpiece increased by increasing material removal volume, regardless of the utilized cutting parameters. This indicates a good self-sharpening effect of the tool. The first three test series clearly show that the roughness decreases with increasing cutting speed because of the reduced chip thickness and increased momentarily active cutting edges. As expected, the last three series showed an increasing roughness trend with increasing the feed rate.

It is noticeable that the roughness values after 300 mm³ material removal are significantly higher than those at lower material removals. Since the cooling channels were designed in two rows, the wear rate of the wheel was much higher at these areas (due to the lower number of abrasives). The nonuniform tool wear resulted in the formation of two raised areas (hills) on the workpiece (Fig.15). It is claimed that an optimized pattern of the cooling holes can prevent this nonuniform wear behavior of the grinding wheel. Fig. 15 shows an overview of ground workpieces with different grinding parameters (cutting speed–feed–material removal volume) and material removal volumes. Clearly, raised areas can be seen at material removal volume of 300 mm³. It is also clear that low cutting speed (15 m/s) led to higher wear rate and faster formation of raised areas on the ground workpiece. Additionally, high feed rate (6000 mm/min) and consequently high material removal rates also induced high tool wear even at higher cutting speeds.

Figure 16 compares the induced surface roughness by both C-50-K and C-50 wheels at different cutting speeds and after 150 mm³ material removal in reciprocating grinding. The roughness in all cases is about the same level of about 2.2 μm. Increasing the cutting speed only slightly optimized the workpiece surface roughness. The reduced volume of abrasives due to the holes on the grinding wheel surface had no negative effect on the surface quality of the workpiece. Slightly enhanced surface quality, i.e. lower surface roughness, were observed in the case of the C-50-K wheel (grinding wheel with cooling channels). It could be due to the positive role of cooling and lubrication in the contact zone, e.g. reduced friction between cutting edges, bond and the workpiece surface, on the workpiece surface quality.

The workpiece surface roughness was also investigated for the deep grinding. Nonuniform worn areas were observed on the C-50-K tool after deep grinding of rather high workpiece material volume. This is again due to the fact that the C-50-K wheel has a large number of cooling channels and therefore not uniformly distributed abrasive grains on its periphery. For this reason, the workpiece surface roughness in deep grinding is only evaluated for C-50 Wheel in Fig. 17.

At a low feed rate of 200 mm/min, rather small roughness values were measured at the beginning of deep grinding process and at low material removal volumes. However, with increasing material removal this value increased. This could be mainly due to the grinding tool's self-sharpening effect. At material removal rates higher than 1.5 mm³/mm.s, i.e. $a_e = 0.1$ mm, $v_{ft} = 1000$ mm/min and $a_e = 0.2$ mm, $v_{ft} = 600$ mm/min, the grinding wheel showed a stable self-sharpening from the first grinding passes and its behavior remained constant until the material removal of 300 mm³. Even after achieving a grinding depth of 0.5 to 1 mm, the aluminum workpiece roughness, Ra, with the grinding wheel C-50 is also in the range of approx. 2.2 μm. This relatively high value is due to the ductile material behavior of aluminum. In comparison, a workpiece was ground from hardened steel (100Cr6, Hardness of 60 HRC).

Figure 18 shows the confocal images of the surface topography for the material 100Cr6 (hardness 60 HRC) and aluminum ground with the C-50-K wheel. The ground surface of the hardened steel has a fine surface structure with a roughness Ra of 0.2 μm. It is important to show that the workpiece material and its hardness significantly influenced the ground surface roughness. Aluminum and hardened steel were ground with the same grinding wheel and grinding parameters. The surface roughness (Ra) was reduced from Ra 1 μm (aluminum) to Ra 0.2 μm (hardened steel). Additionally, an experiment with a specific material removal volume up to $V'w = 500$ mm³/mm (long term experiment) was performed with the C-50-K wheel and constant grinding parameters at a specific material removal rate of $Q'w = 0.33$ on the hardened steel (100Cr6 60HRC). The obtained G-ratio (the ration of removed workpiece material to the worn volume of the grinding wheel) was about 6. Compared to the G-ratio of 1.3 reported in [26] for Al₂O₃ grinding wheels with the same grain size F220, this additive manufactured grinding wheel shows an excellent potential for the manufacturing process.

In Fig. 19 the microscopic images of the additive manufactured grinding wheels with and without cooling lubricant channels after the grinding experiments on hardened steel 100Cr6 with similar cutting parameters are shown. After a few grinding cycles, large loading areas on the surface of grinding wheel

C-50 were detected. In contrast, the C-50-K grinding wheel (with cooling lubrication channels) experienced almost no tool loading.

Tool loading is the adhesion of the layers of workpiece material, i.e. chips, to the tool surface. Tool loading changes the micro-topography of the grinding wheel and therefore causes high friction that leads to an increase in grinding forces and temperature in the contact zone between the tool and the workpiece. Furthermore, tool loading impacts geometry and profile deformation and deteriorated workpiece surface quality. In order to avoid such problems, in industrial applications either cooling lubrication should be optimised [22] or grinding wheels are dressed at certain intervals [24,25]. By integrating cooling lubricant channels into the C-50-K grinding wheel, the coolant delivery could be improved. Hence, a better cooling in the contact zone could be obtained and thus grinding forces and temperature could be reduced, therefore, tool loading was prevented. A stable grinding process could be achieved which would increase the surface quality and the process efficiency.

3.4 Influence of grain concentration

For the investigation of the influence of the grain concentration in the resin bond, an additive grinding wheel with 25 wt.% of SiC F220 and having the same coolant channels as the C-50-K wheel was printed. Comparative experiments of 25% and 50% grain contents regarding workpiece surface quality and tool wear were carried out accordingly. The results for different cutting parameters, i.e. cutting and feed speed, depth of cut and material removal volume, are summarized in Fig. 20.

For all cutting parameters, the grinding wheel with a higher grain concentration (50 wt.%) showed better grinding performance. With doubled grain concentration, the surface roughness was reduced to about half. In processes with high feed rate or high depth of cut and thus a high material removal rate (Fig. 20 last four settings), the differences in grinding wheels wear are clearly visible. Due to an increased amount of the abrasive grains, the tool wear has been reduced between 3 to 30 times. The increased number of abrasive grains on the tool surface increase the effective hardness of the wheel and reduces the chip thickness and acting loads on each active grain during the material removal process. Additionally, the reduced chip thickness due to the higher amount of abrasives caused a reduction in the surface roughness of the workpiece.

4. Conclusions

Using DLP-based additive manufacturing, resin bonded grinding tools consisting of SiC grains and photopolymers were successfully printed layer by layer. In this liquid printing process, the abrasive grains were well mixed and embedded in the UV resin (ultraviolet light-curable resin) without accumulation. This novel manufacturing process allows grinding wheels with any geometry and special features to be produced easily, quickly and economically. Surface grinding experiments with different cutting parameters were carried out to evaluate the grinding efficiency of the additive manufactured grinding wheels and the results are summarized below.

In deep grinding experiments and at constant cutting parameters, the observed wear of the grinding wheel with cooling channels was always less than that without cooling channels. Particularly in the contact zone, where a lot of heat is generated in the grinding process, the coolant channels show a positive influence, as they are able to transfer the heat easily. This also results in a lower grinding force compared to grinding wheels without cooling channels.

Grinding experiments on hardened steel 100Cr6 showed that the integration of cooling lubricant channels increases the amount of coolant delivered to the contact zone. Due to the improved lubrication and cooling in the contact zone, tool loading could almost be prevented. This led to a stable and efficient grinding process. However, these cooling channels in some cases in shallow reciprocating grinding did not improve the grinding process.

The C-50-K grinding wheel underwent non-uniform wear at high material removal volumes and caused raised areas on the workpiece surface. Hence, arrangement and number of cooling channels should be adapted and optimized in order to achieve the positive influence on the grinding process and at the same time a high stability of the wheel.

In addition to the quantitative evaluation and systematic analysis of the grinding performance of the additive manufactured grinding wheels as a function of geometry (with and without cooling lubricant channels), the cutting parameters (cutting speed, feed rate, depth of cut) as well as the specification of the grinding wheel (grain content 25 wt.% and 50 wt.% SiC grains) were investigated. By increasing the cutting speed and decreasing the feed rate, the wear of the grinding wheels was significantly reduced. The surface roughness (Ra) of the ground aluminum sample was in the range between 1 μm and 2.5 μm , whereas it was approximately 0.2 μm for the hardened steel specimen. In all process settings, the grinding wheel with the higher grain concentration of 50%.wt showed a significantly more efficient process (lower surface roughness and less grinding wheel wear). Therefore, the grit concentration has a great influence on the performance of additive manufactured grinding wheels.

Using a novel digital image processing system, the surface topography of the grinding tools was scanned and analyzed to detect the wear characteristics such as flattened abrasive grains. Significant correlations between the obtained surface topography of flattened grains and the increase in grinding forces due to the tool wear were observed.

In this study the influences of the cooling channels as well as the grain type were only studied in a limited extent. The grinding wheel composition can be varied easily by the DLP process and can be adapted to the requirements of the specific application. Depending on the application, a corresponding grain content can be mixed in and printed. The pattern and number of cooling channels and tool specification will be the subject of further studies.

Declarations

Acknowledgments

The author would like to thank the “ministry for science, research and the arts of Baden-Württemberg” for the financial support of the project “AddiGrind” and the company Diamant-Gesellschaft Tesch GmbH for the partly financial support and providing the required materials.

Funding

This project “AddiGrind” was funded by the Ministry of Science, Research and the Arts of the State of Baden-Wuerttemberg. Partial financial and material support was received from company Diamant-Gesellschaft Tesch GmbH.

Author Contributions

Qingfeng Ai: conceptualization, writing, research, investigation.

Jahangir Khosravi: investigation, editing.

Bahman Azarhoushang and Amir Daneshi: methodology, reviewing, project administration.

Björn Becker: investigation, software

Corresponding author: Qingfeng Ai

Competing Interests

The authors have no relevant financial or non-financial interests to disclose and have no competing interests.

Ethical approval

This paper is new and has not been published, accepted or submitted to any other journal.

Consent to participate

Not applicable

Consent to publish

Not applicable

Availability of data and materials

The manuscript has no associated data or materials

References

- [1] Habrat WF. Effect of Bond Type and Process Parameters on Grinding Force Components in Grinding of Cemented Carbide. *Procedia Engineering* 2016;149:122–9. <https://doi.org/10.1016/j.proeng.2016.06.646>.
- [2] Linke B. Manufacturing and sustainability of bonding systems for grinding tools. *Production Engineering* 2016;10(3):265–76. <https://doi.org/10.1007/s11740-016-0668-5>.
- [3] Kirsch B, Aurich JC. Influence of the Macro-topography of Grinding Wheels on the Cooling Efficiency and the Surface Integrity. *Procedia CIRP* 2014;13:8–12. <https://doi.org/10.1016/j.procir.2014.04.002>.
- [4] Azarhoushang B, Zahedi A. Laser conditioning and structuring of grinding tools – a review. *Advances in Manufacturing* 2017;5(1):35–49. <https://doi.org/10.1007/s40436-016-0167-0>.
- [5] Azarhoushang B, Rasifard A. Das Abrichten als integraler Bestandteil des Schleifprozesses: Mechanische Abrichtprozesse. *diamond business* 2014;49:64–71.
- [6] Walter C, Komischke T, Kuster F, Wegener K. Laser-structured grinding tools – Generation of prototype patterns and performance evaluation. *Journal of Materials Processing Technology* 2014;214(4):951–61. <https://doi.org/10.1016/j.jmatprotec.2013.11.015>.
- [7] Bikas H, Koutsoukos S, Stavropoulos P. A decision support method for evaluation and process selection of Additive Manufacturing. *Procedia CIRP* 2019;81:1107–12. <https://doi.org/10.1016/j.procir.2019.03.261>.
- [8] Tian C, Li X, Shubo Z, Guo G, Wang L, Rong Y. Study on design and performance of metal-bonded diamond grinding wheels fabricated by selective laser melting (SLM). *Materials and Design* 2018;156:52–61. <https://doi.org/10.1016/j.matdes.2018.06.029>.
- [9] Yang Z, Zhang M, Zhang Z, Liu A, Yang R, Liu S. A study on diamond grinding wheels with regular grain distribution using additive manufacturing (AM) technology. *Materials & Design* 2016;104:292–7. <https://doi.org/10.1016/j.matdes.2016.04.104>.
- [10] Du Z-j, Zhang F-l, Xu Q-s, Huang Y-j, Li M-c, Huang H-p et al. Selective laser sintering and grinding performance of resin bond diamond grinding wheels with arrayed internal cooling holes. *Ceramics International* 2019;45(16):20873–81. <https://doi.org/10.1016/j.ceramint.2019.07.076>.
- [11] J. Hajduk JM. Resin Bonded Grinding Wheel: U.S. Patent; 2014; Available from: <https://patents.google.com/patent/US20140057534A1/en>.
- [12] Guo L, Huang Q, Marinescu I. Effect of nanosized alumina fillers on manufacturing of UV light-curable-resin bond abrasive tool. *Machining Science and Technology* 2017;21(2):223–38. <https://doi.org/10.1080/10910344.2017.1283961>.
- [13] Pappas SP. *Radiation Curing: Science and Technology*. Springer US; 2013.

- [14] Bajpai M, Shukla V, Kumar A. Film performance and UV curing of epoxy acrylate resins. *Progress in Organic Coatings* 2002;44:271–8. [https://doi.org/10.1016/S0300-9440\(02\)00059-0](https://doi.org/10.1016/S0300-9440(02)00059-0).
- [15] Chattopadhyay D, Panda S, Kothapalli RV. Thermal and mechanical properties of epoxy acrylate/methacrylates UV cured coatings. *Progress in Organic Coatings* 2005;54:10–9. <https://doi.org/10.1016/j.porgcoat.2004.12.007>.
- [16] Huang Q, Guo L, Marinescu ID. Research on the Properties of Resin Bond Wheel Cured by Ultraviolet Light. *Procedia Manufacturing* 2016;5:259–69. <https://doi.org/10.1016/j.promfg.2016.08.023>.
- [17] Marinescu I, Guo L, Wei P. Basic Research for the UV Fixed Abrasive Lapping Plate. *Applied Mechanics and Materials* 2013;371:95–100. <https://doi.org/10.4028/www.scientific.net/AMM.371.95>.
- [18] L. Guo, X. Zhang, C. Lee, I. D. Marinescu, Y. Zhang, J. Hui. An Experimental Study on the Abrasive Machining Process of Electronic Substrate Material With A Novel Ultraviolet-Curable Resin Bond Diamond Lapping Plate. *IEEE Access* 2019;7:64375–85. <https://doi.org/10.1109/ACCESS.2019.2917304>.
- [19] Qiu Y, Huang H, Xu X. Effect of additive particles on the performance of ultraviolet-cured resin-bond grinding wheels fabricated using additive manufacturing technology. *The International Journal of Advanced Manufacturing Technology* 2018;97(9):3873–82. <https://doi.org/10.1007/s00170-018-2231-3>.
- [20] Tanaka T, Isono Y. New development of a grinding wheel with resin cured by ultraviolet light. *Journal of Materials Processing Technology* 2001;113(1):385–91. [https://doi.org/10.1016/S0924-0136\(01\)00636-7](https://doi.org/10.1016/S0924-0136(01)00636-7).
- [21] Verkerk J. Wheelwear control in grinding: models for the control of wheelwear, grinding force and surface roughness by the choice of dressing and grinding conditions 1976.
- [22] Ludwig S, Azarhoushang B (eds.). *In-process grinding wheel wear evaluation using digital image processing*; 2018.
- [23] Azarhoushang B. *Intermittent Grinding of Ceramic Matrix Composites: Unterbrochenes Schleifen von keramischen Faserverbundwerkstoffen*. 1st ed. Aachen: Shaker; 2011.
- [24] Azarhoushang B, Luckstein T, Zahedi A. Erzeugung von Mikro-strukturen auf einer cBN-Schleifscheibe mit einem Pikosekundenlaser. *DIHW* 2014:40–5.
- [25] König W. *Fertigungsverfahren*. 4th ed. Berlin: Springer; 2005.
- [26] Badger J, Murphy S, O'Donnell GE, Big-and-dull or small-and-sharp: A comparison of specific energy, wheel wear, surface-generation mechanisms and surface characteristics when grinding with Al₂O₃ and CBN to achieve a given surface roughness, *Journal of Materials Processing Tech.* (2020), doi: <https://doi.org/10.1016/j.jmatprotec.2020.116825>

Figures



Figure 1

Microscopic image of utilized SiC grains

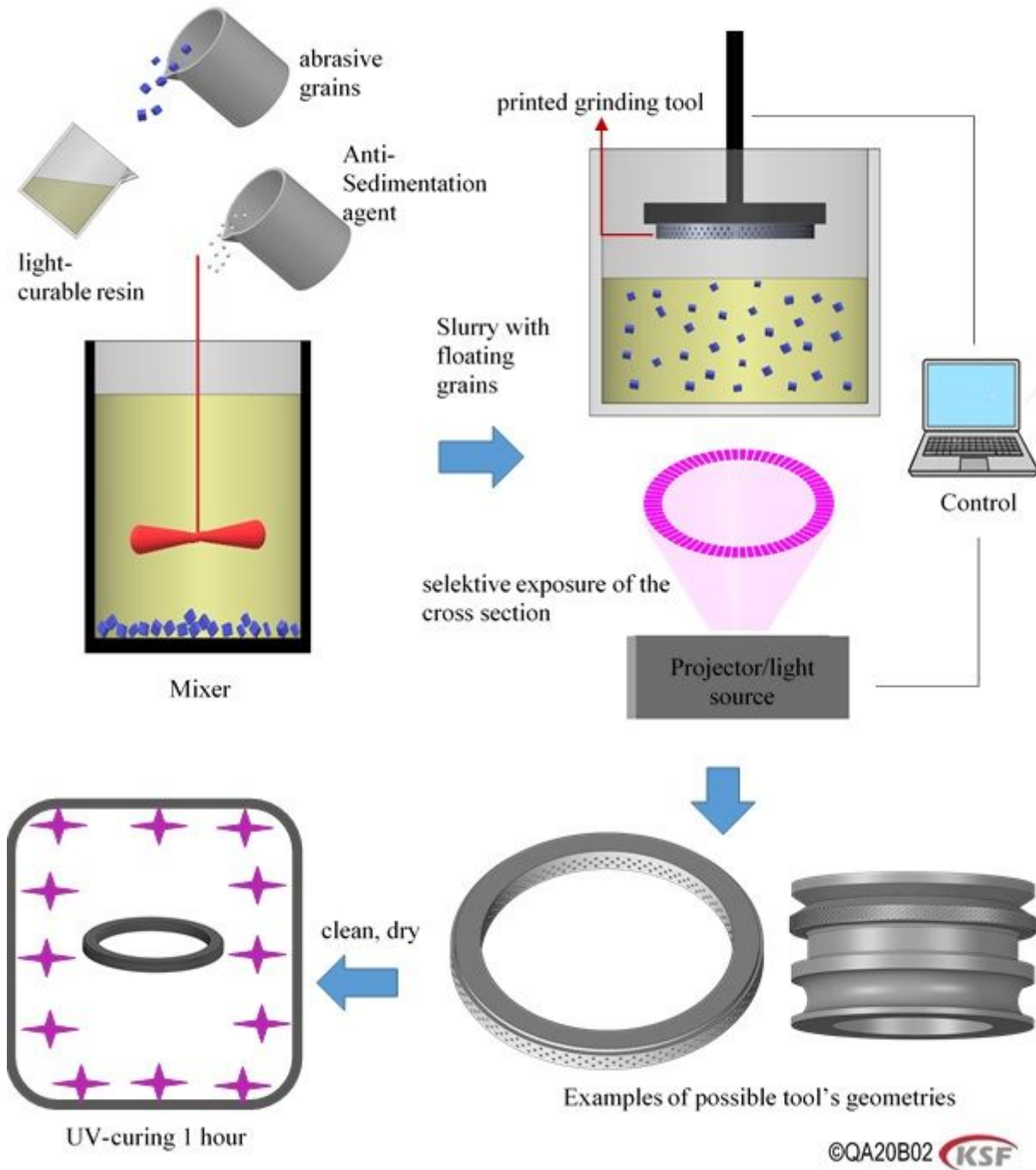


Figure 2

Schematic diagram of DLP-printing and curing processes of the ultraviolet-curable resin bonded abrasive tools

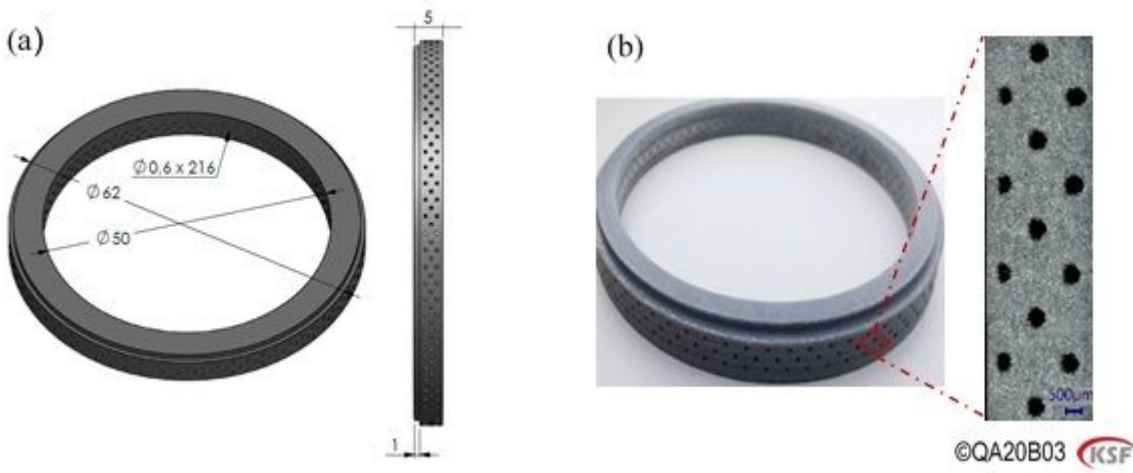


Figure 3

Structure of the printed rim of the grinding wheel: (a) 3D and 2D drawings of the wheel with internal cooling holes (b) Image of 3D printed grinding wheel with internal cooling holes



Figure 4

the experimental setup

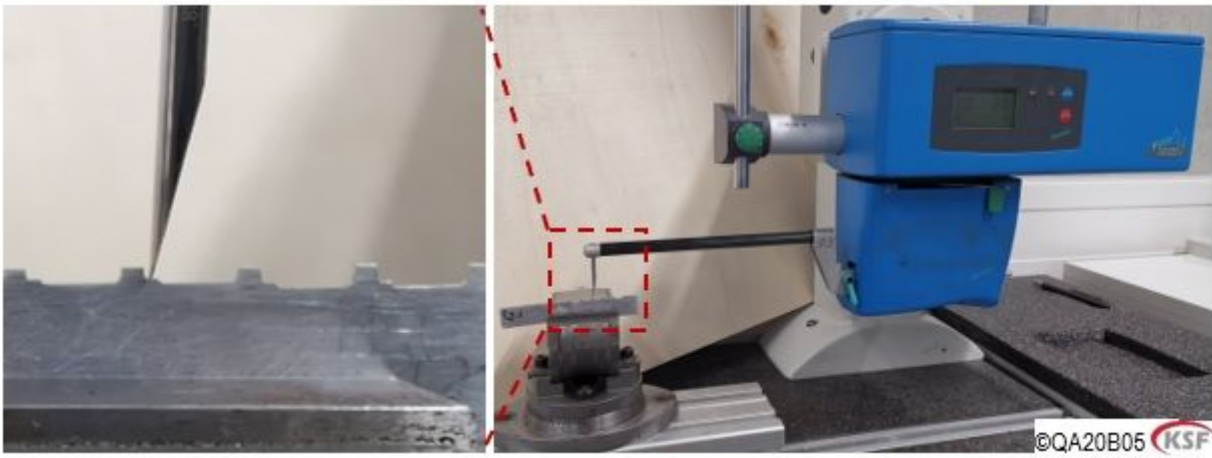


Figure 5

wear measuring with a stylus ((Hommel-Werke: T-8000)

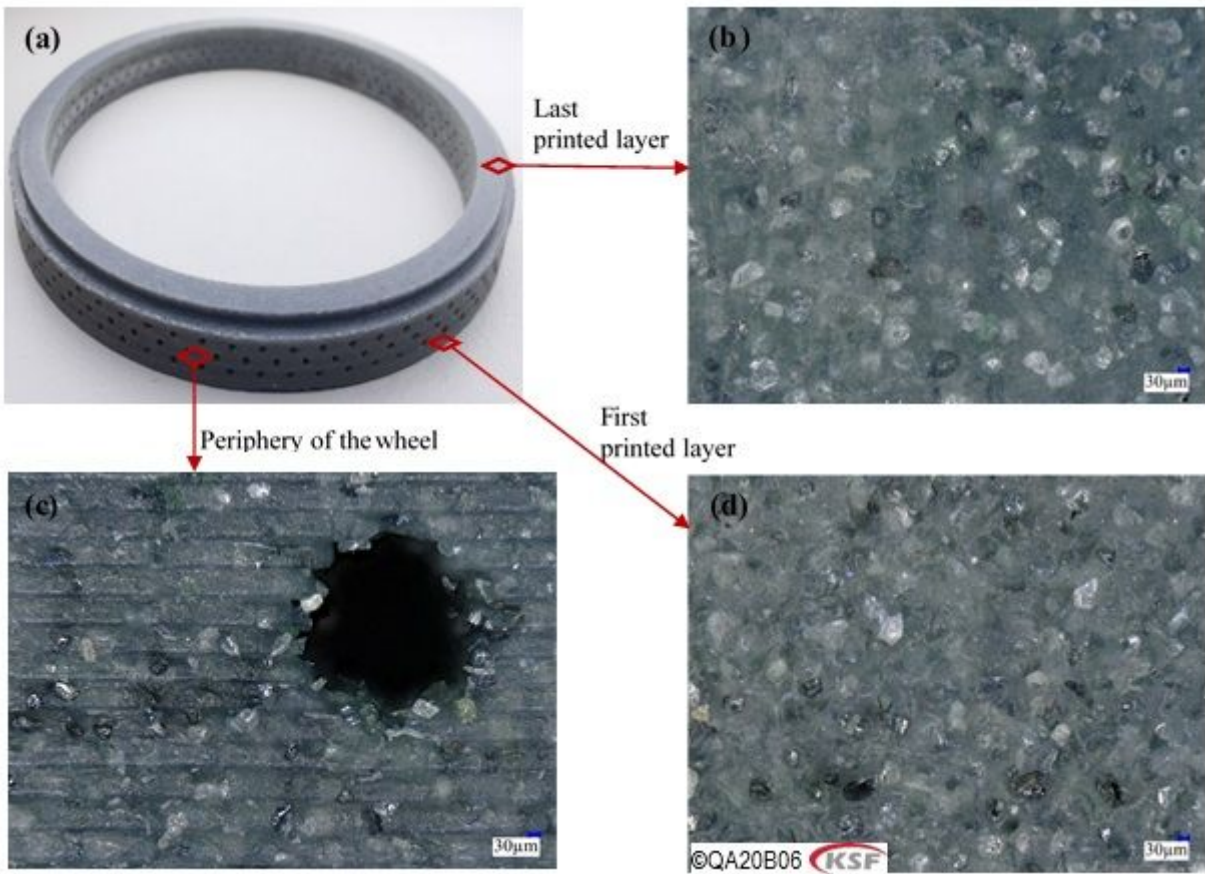


Figure 6

(a) the additive-manufactured resin-bonded grinding wheel with 25 wt.% silicon carbide F220 grains; (b) optical microscope photo from the last printed layer; (c) the periphery of the grinding wheel with 200x magnification; (d) the first printed layer

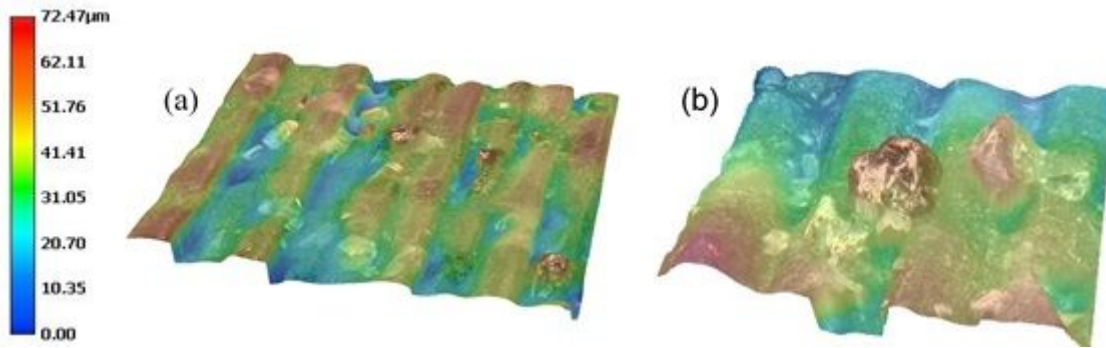


Figure 7

Topography of the 3d-printed grinding tools (confocal microscopy)



Figure 8

the coolant is almost tangentially positioned to the grinding wheel and sprayed out of the internal cooling channels of the 3D-printed grinding tool

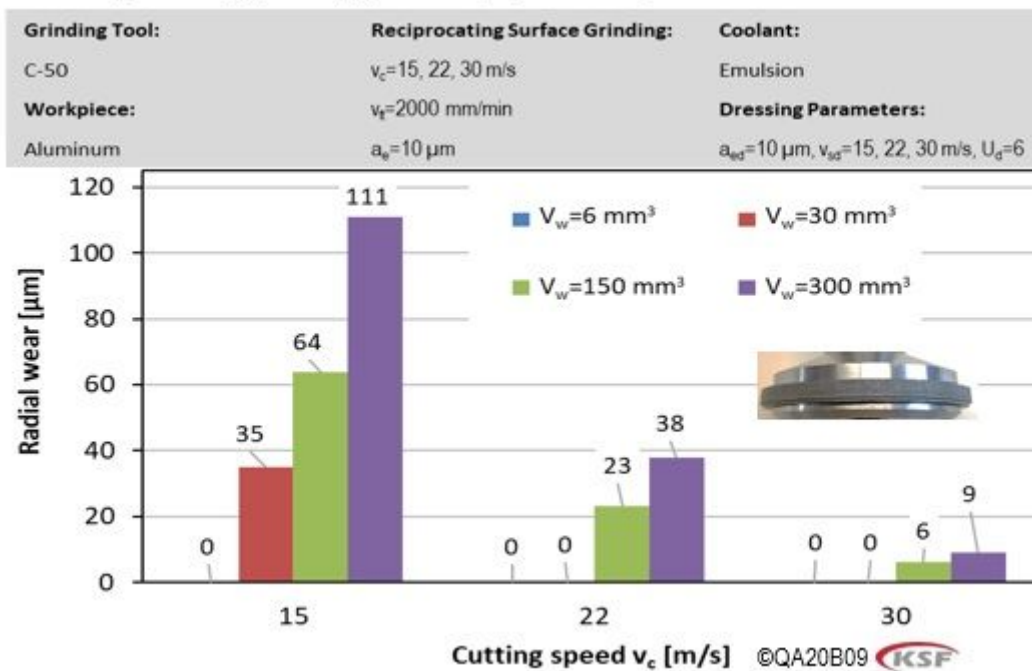


Figure 9

Radial wear values of the C-50 printed wheel at various cutting speeds, v_c , and material removal volumes, V_w

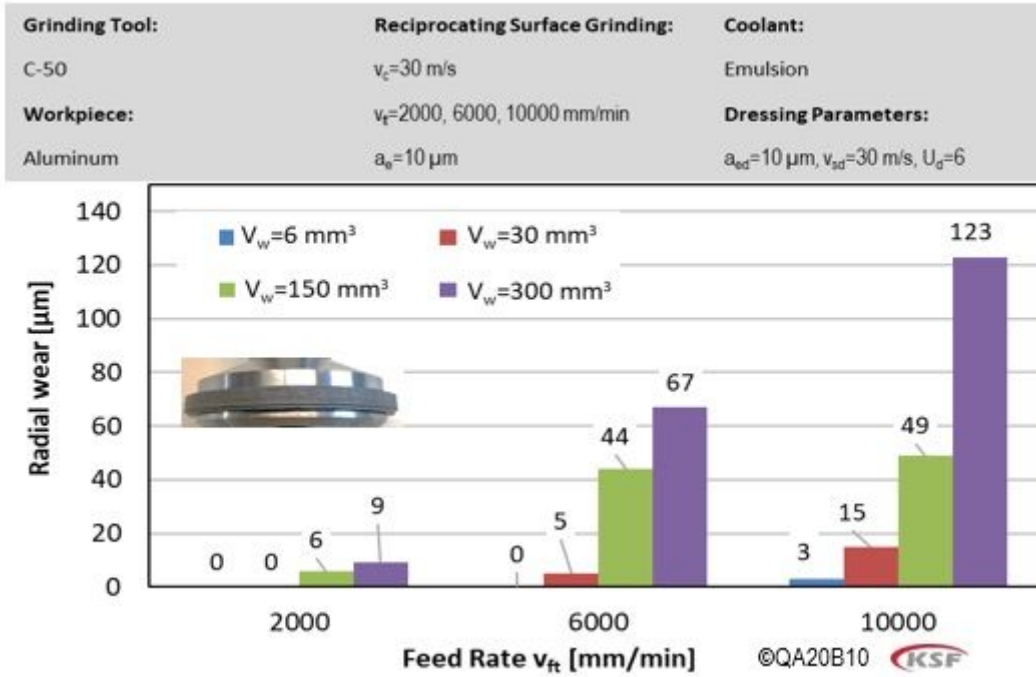


Figure 10

Radial wear values of the C-50 printed wheel at various feed rates, v_{ft} , and material removal volumes, V_w

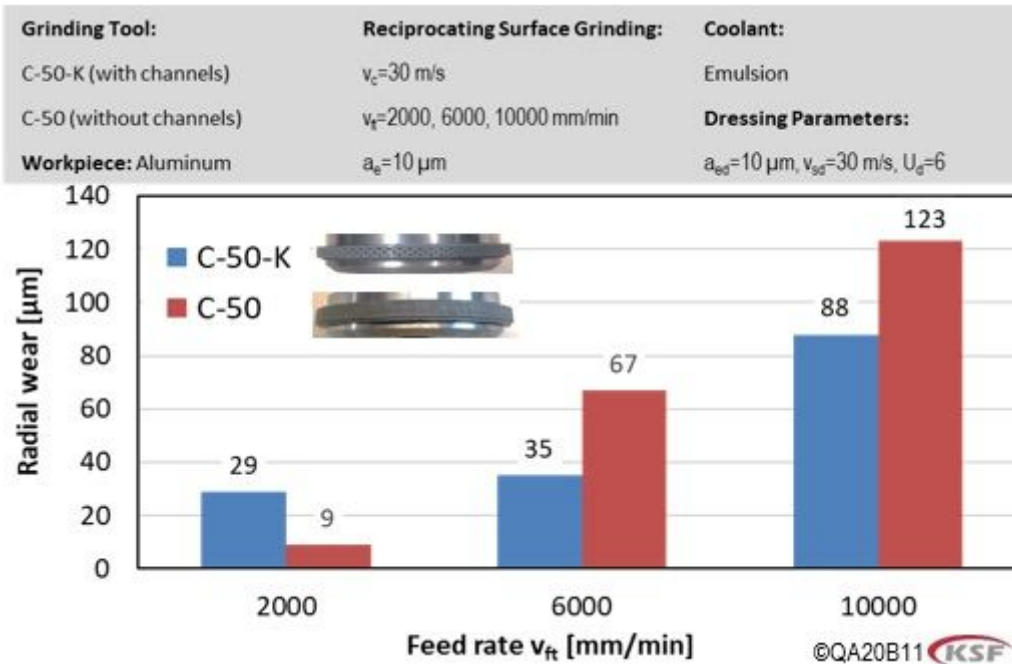


Figure 11

A comparison between the radial wear of C-50-K and C-50 wheels in reciprocating grinding of aluminum after 300 mm³ material removing

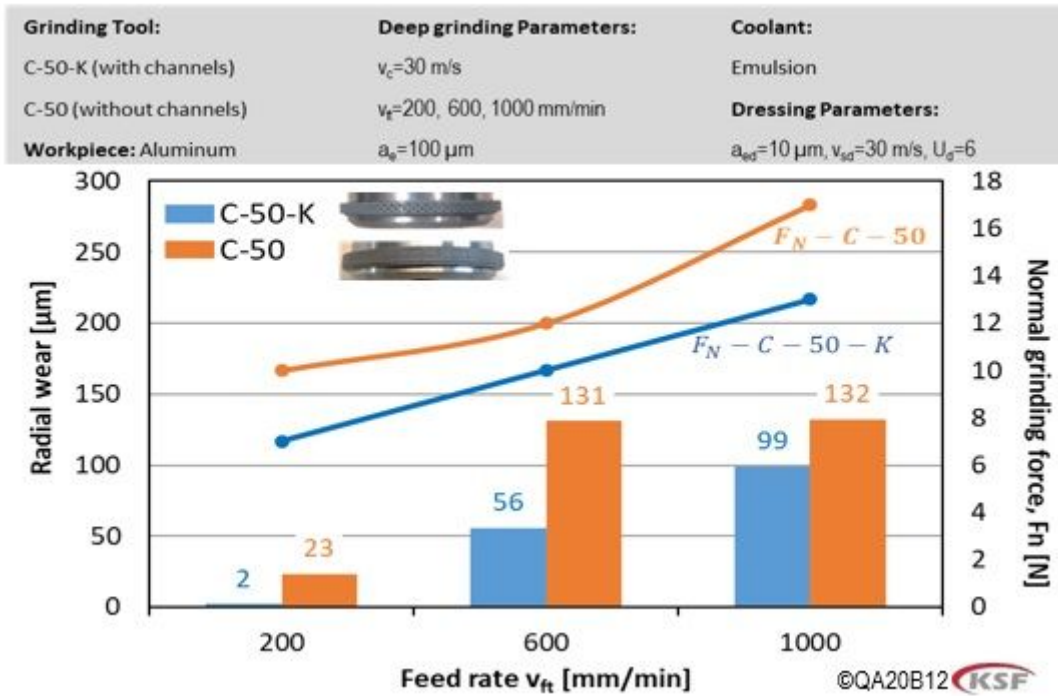


Figure 12

Radial tool wear and normal grinding force in grinding by the tools with and without cooling lubricant channels versus the feed rate

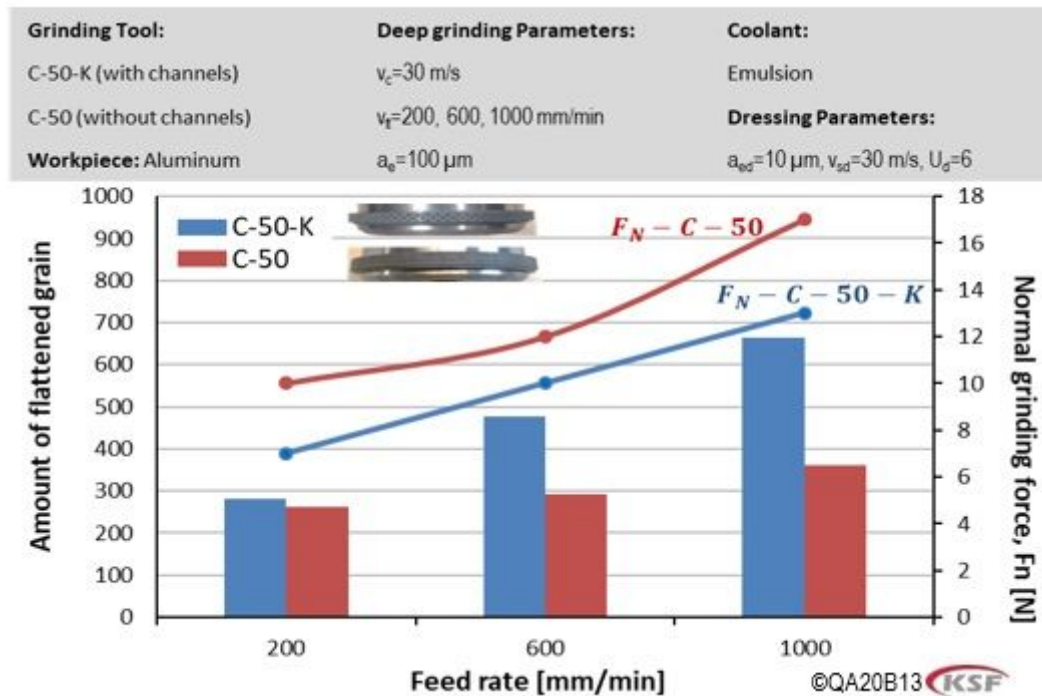


Figure 13

The number of reflections (amount of flattened grains) in connection with the grinding forces for C-50 and C-50-K wheels at different feed rates

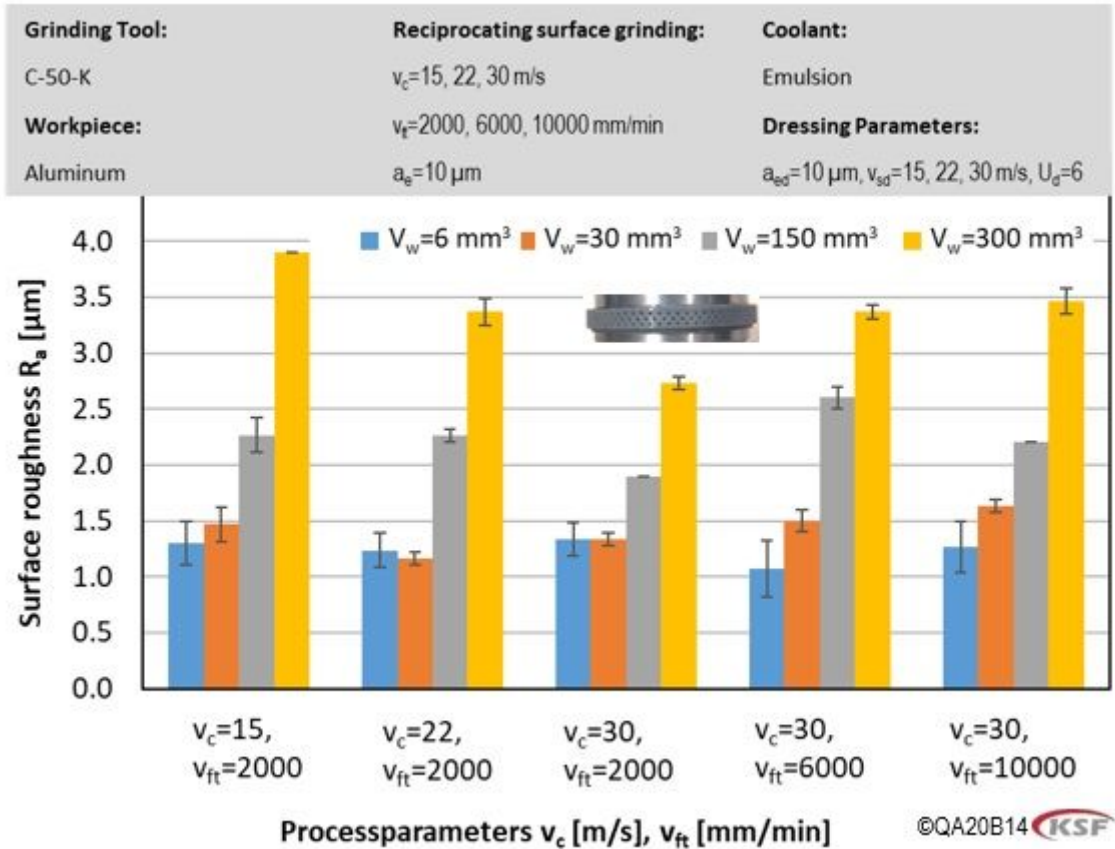


Figure 14

Surface roughness for different process parameters

v_c [m/s] – v_{ft} [mm/min] – V_w [mm³]

©QA20B15 

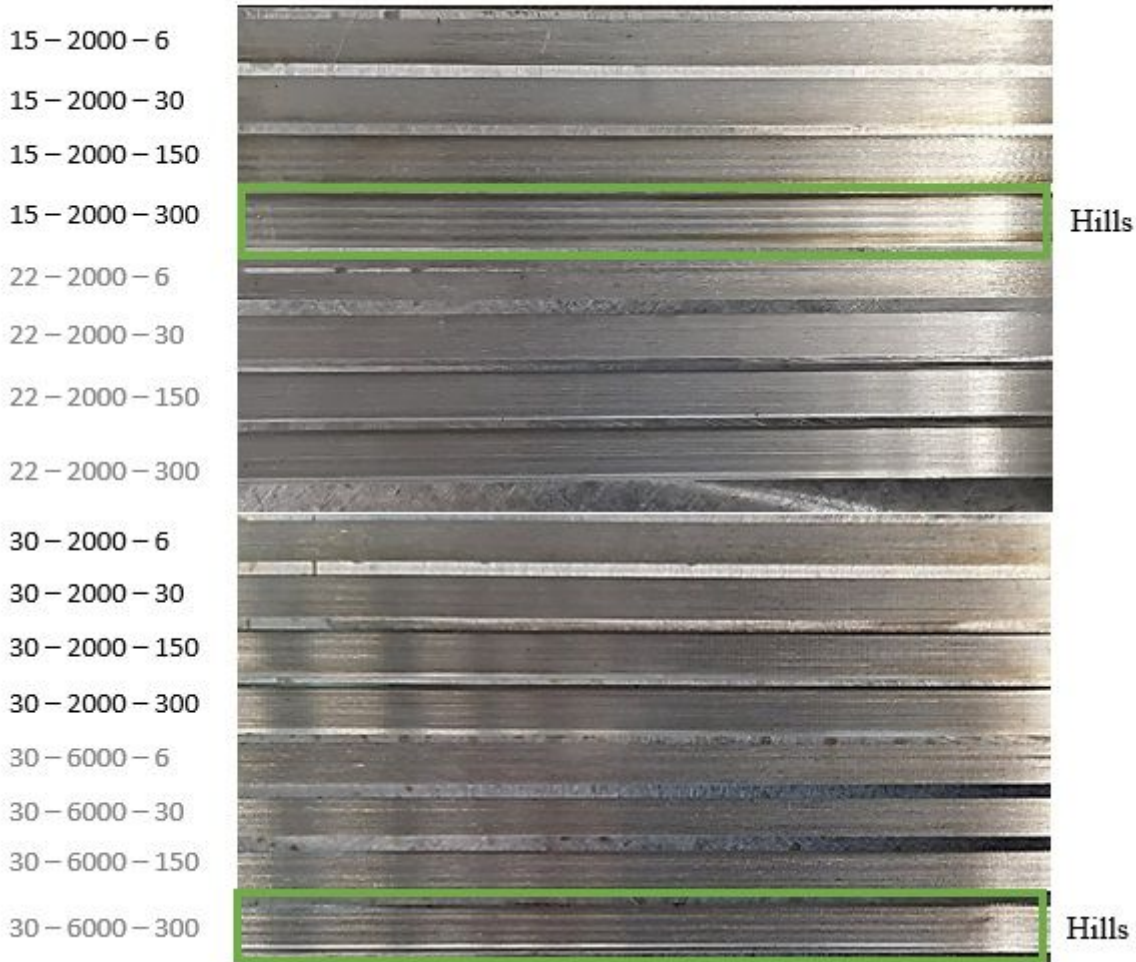


Figure 15

Ground grooves with different cutting speeds, feed rate and material removal volumes, and at a constant depth of cut of 10 μm . The nonuniform tool wear at rather high material removal volumes resulted in the formation of two raised areas on the workpiece

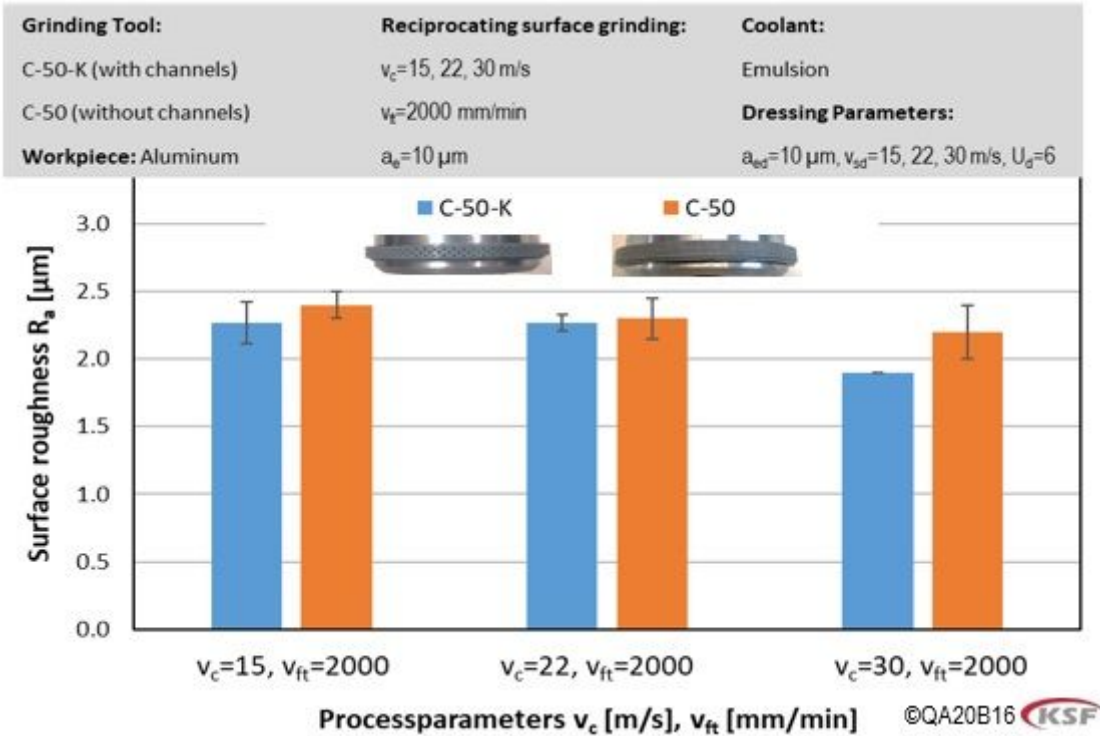


Figure 16

Comparison of the surface roughness at different cutting speeds and for 3D-printed grinding wheels with and without coolant channels

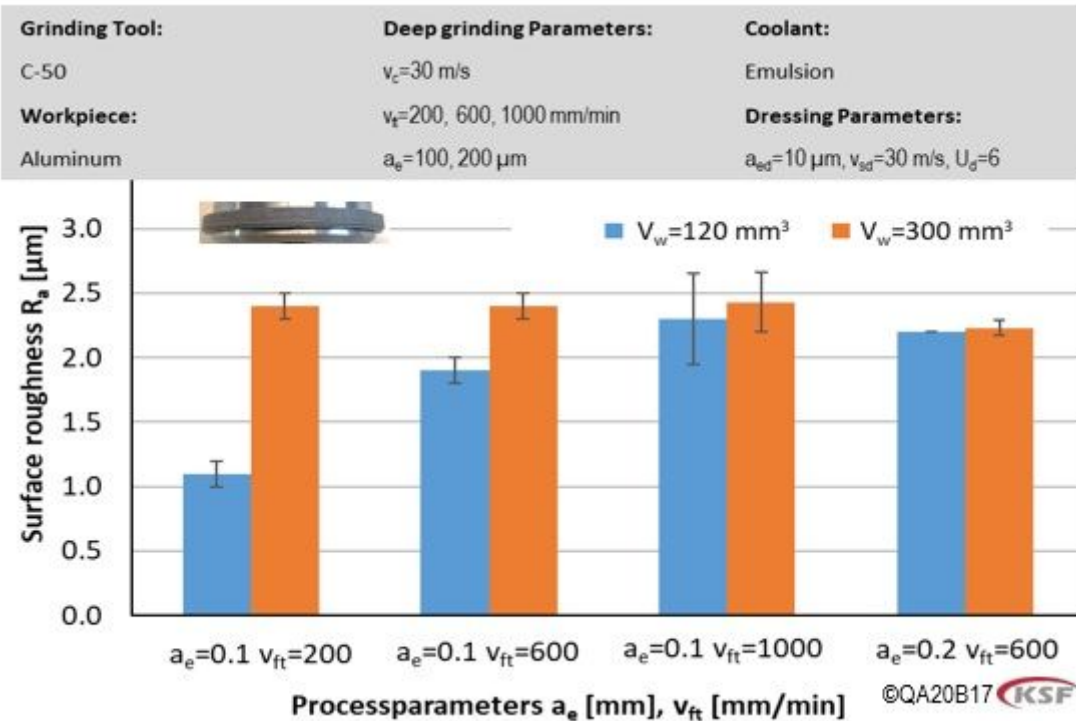


Figure 17

The effect of cutting parameters on the surface roughness

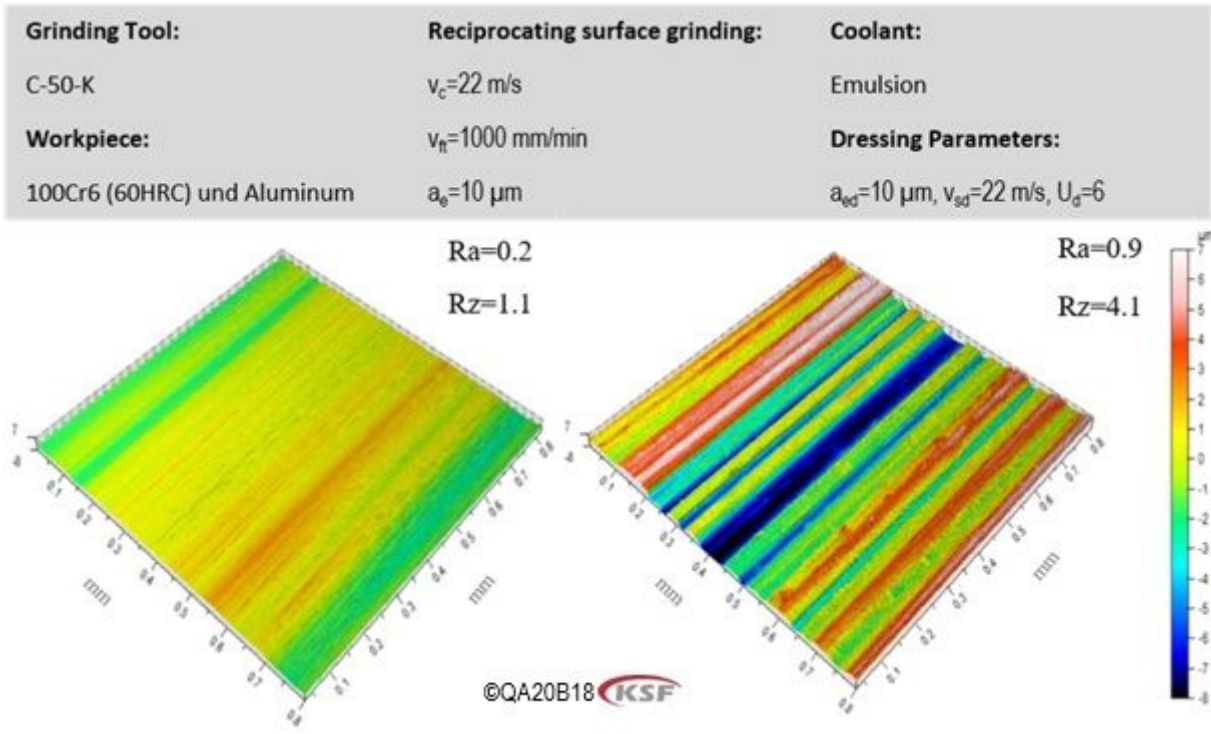


Figure 18

Surface topography for the material 100Cr6 (hardness 60 HRC) and aluminum

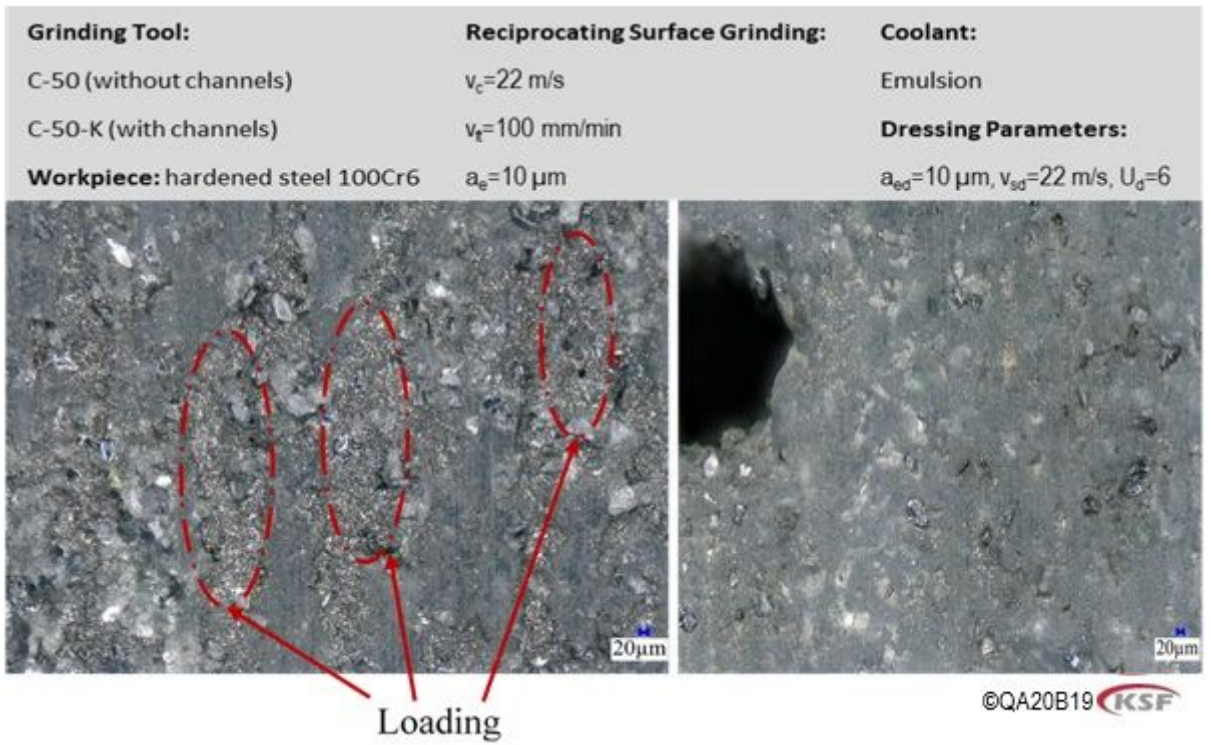


Figure 19

Microscopic images of the additive manufactured grinding wheels without (left) and with cooling lubricant channels (right) after the grinding experiments on hardened steel 100Cr6

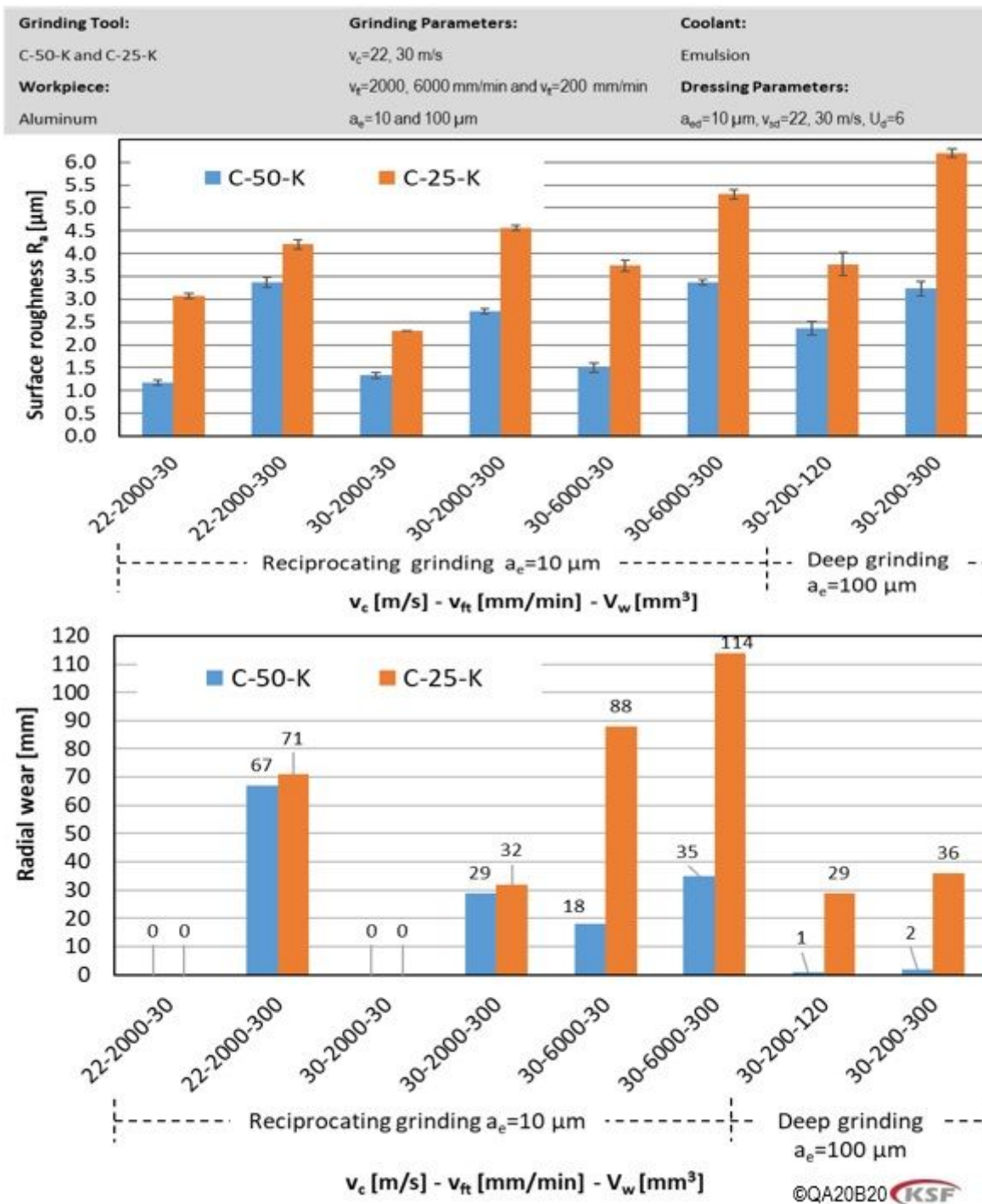


Figure 20

comparison of the surface roughness and the tool wear for grinding wheels with concentration 25 wt. % and 50 wt. % at different cutting parameters